Europium-doped $NaGd(WO_4)_2$ nanophosphors: synthesis, luminescence and their coating with fluorescein for pH sensing

Mariano Laguna, Alberto Escudero, Nuria O. Núñez, Ana I. Becerro and Manuel Ocaña*

Instituto de Ciencia de Materiales de Sevilla, CSIC, Américo Vespucio 49, 41092, Isla de la Cartuja, Sevilla, Spain

*Corresponding author: mjurado@icmse.csic.es

Abstract

Uniform Eu-doped $NaGd(WO_4)_2$ nanophosphors having spherical shape have been synthesized for the first time by using a wet chemistry method based on a homogeneous precipitation process at low temperature (120ºC) in ethylene glycol/water mixtures. The obtained nanoparticles crystallized into the tetragonal structure and presented polycrystalline character. The europium content in such phosphors has been optimized through the analysis of the luminescence dynamics (lifetime measurements). By coating the Eu^{3+}-doped wolframate based nanoparticles with fluorescein through a layer-by-layer (LbL) approach, a wide range (4-10) ratiometric pH-sensitive sensor has been developed, which uses the pH insensitive emission of Eu^{3+} as reference.

1. Introduction

Nowadays, rare earth (RE) based phosphors consisting of a large variety of compounds containing active lanthanide (Ln) cations are being subject of much research because of their important technological applications in the optoelectronic (photovoltaic cells, plasma display panels, lighting, etc.)[1-3] and more recently, the biotechnological fields (sensors, imaging, therapy, etc.).[4] These research activities have been mainly justified on the basis of the advantageous characteristics of such materials when compared with other luminescent compounds such as quantum dots, which include high chemical and thermal stability, high luminescence efficiency and low toxicity. They suffer however from a main drawback related to the low intensity of their emissions, which is due to the low absorption coefficient associated to the electronic transitions involved in the luminescence process of the Ln cations.[5] One of the suggested approaches to increase the intensity of such emissions is based on an energy transfer mechanism. Essentially, it consists of the absorption of energy by certain inorganic anions having an adsorption coefficient much larger than that of Ln ions, which is further transferred to the latter thus increasing the intensity of their luminescence.[5] One of the most efficient anions for such a purpose is tungstate (WO_4^{2-}).[6] In fact, a large variety of phosphors consisting of tungstate containing matrices doped with Ln^{3+} cations have been developed having applications in lasers,[7] temperature sensing[8] and lighting devices,[9] to mention a few. However, very little attention has been paid to the potential biotechnological applications of these phosphors,[10] which is probably due to the scarcity of preparation methods able to produce uniform and well dispersed nanoparticles (NPs) of such compounds, which are required for this kind of uses.[11] In fact, up to our knowledge, uniform $NaGd(WO_4)_4$ nanoparticles have been only synthesized at high (300ºC) temperature through a

precipitation method using oleic acid as capping agent which results in hydrophobic nanoparticles.[12]

A particular case of biosensors are those developed for pH sensing. These have been shown to be very useful for studies related to NPs uptake by cells, since they can discriminate between acidic endosomal/lysosomal and neutral extracellular environment.[13] For this application, ratiometric sensors are desired, since in this case, the analysis is independent on the local fluorophore concentration.[14] Different ratiometric systems can be found in the literature, including single dyes and nanostructures conjugated with pH-sensitive dyes. Seminaphtharhodafluor (SNARF) is an organic fluorophore widely used as pH sensor for ranges between 6.5 and 9.[15] It shows two different emissions whose intensity ratio is pH sensitive. Since SNARF itself does not enter cells,[16] it is normally attached to colloids, such as plasmonic NPs,[17] or loaded in micrometric capsules,[15, 18-19] that act as carrier. For other pH ranges, different pH-sensitive fluorophores can be attached to luminescent NPs, and the intrinsic emission of the latter can be used as the reference signal. The attachment of fluorophores to NPs can be advantageous, since higher chemical and fluorescence stabilities and sensitivities are normally observed.[14] Such strategy has been used with both quantum dots and RE-based NPs. Thus, quantum dots functionalized with Oregon Green (OG) have been used for pH sensing in a range between 3.5 and 6,[20] and Yb^{3+}, Er^{3+}-doped $NaYF_4$ upconversion NPs functionalized with porphyrins have been reported to show a good pH response for the pH range between 6 and 8.[21] Wider pH ranges can be sensed with more complex systems based on polyacrylamide-based NPs functionalized with three fluorophores (Oregon Green, fluorescein, and the pH-insensitive rhodamine B, which acts as reference) covering a pH range from 3.2 to 7.[22] We have recently developed a much simpler wide-range pH (from 4 to 11) sensor, based on Eu^{3+}-doped rare earth (Y, Gd) vanadate NPs

conjugated with Nile Blue.[23] It has to be mentioned that for the preparation of such sensor, the Nile Blue conjugation requires the presence of carboxylate groups on the NPs surface for which, the latter had to be previously functionalized with polyacrylic acid.

In this work, we have developed a procedure for the synthesis of uniform nanospheres of europium doped $NaGd(WO_4)_2$ based on a homogeneous precipitation process at low temperature (120ºC) in polyol/water mixtures. The Eu concentration has been optimized through the analysis of the luminescence dynamics (lifetime measurements). With these nanophosphors we have also developed a wide range (4-10) pH-sensitive nanosensor by coating the Eu^{3+}-doped wolframate based NPs with fluorescein, a fluorescent dye with a pH-dependent emission.[24-25] In this case, the pH insensitive emission of Eu^{3+} is used as reference. Such nanosensor has been prepared by following a facile procedure based on a Layer-by-Layer (LbL) approach,[26-28] which has been carried out using poly(fluorescein isothiocyanate allylamine hydrochloride), a commercially available positively charged polyelectrolyte. It is noticeable that such approach is very simple since a previous NPs functionalization with reactive anchors is not required providing that negatively charged NPs are available.

2. Experimental

2.1. Reagents: Gadolinium (III) nitrate hexahydrate ($GdNO_3 \cdot 6H_2O$, Aldrich, 99.9%) and europium (III) nitrate pentahydrate ($Eu(NO_3)_3 \cdot 5H_2O$, Aldrich, 99.9%) were selected as Ln precursors and sodium tungstate dihydrate ($Na_2WO_4 \cdot 2H_2O$, Aldrich, ≥99%) was used as tungstate source. Sodium citrate (Na_3Cit, $Na_3C_6O_7H_5.2H_2O$, Aldrich, 99.5%) was also needed as complexing agent whereas ethylene glycol (EG, Aldrich, ≥99.5%)-water (Milli-Q) mixtures were used as solvent. Poly(fluorescein isothiocyanate allylamine hydrochloride) (PAH, Mw ~ 15000 Da, Aldrich) and sodium chloride (NaCl, Roth, >99.9%) were used for the preparation of the pH-sensitive nanosensors.

2.2. Synthesis of $NaGd(WO_4)_2$ nanoparticles: The procedure for the synthesis of $NaGd(WO_4)_2$ nanoparticles was as follows. Weighted amounts of $Gd(NO_3)_3$ and sodium citrate were dissolved in a certain volume of Milli-Q water (from 0.5 to 2 cm^3) to form a citrate-Ln complex, and then ethylene glycol was added to this aqueous solution until completing 2.5 cm^3 of the mixture. In a separate vial, the desired amount of Na_2WO_4, was dissolved in ethylene glycol (2.5 cm^3) under magnetic stirring while heating the vial at ~80ºC to facilitate the dissolution process. The resulting solution was left to cool down to room temperature. The latter was then added to the solution containing the Ln-citrate complex, under magnetic stirring, and the mixture was quickly introduced in an oven preheated at 120ºC where it was finally aged for 20 h in tightly closed test tubes. After aging, the resulting dispersions were cooled down to room temperature, centrifuged, and the supernatants were discarded. The precipitates were then washed, twice with ethanol and once with double distilled water and finally redispersed in Milli-Q water. For some analyses, the powders were dried at room temperature.

2.3. Synthesis of Eu-doped $NaGd(WO_4)_2$ nanoparticles. For the synthesis of Eu-doped $NaGd(WO_4)_2$ nanoparticles, we proceeded as described above for the case of the undoped system but incorporating the desired amount of Eu to the starting $Gd(NO_3)_3$ solution. The Eu/(Eu+Gd) molar ratio was varied from 3 to 18% in order to investigate the effect of these doping level on the luminescent properties of the precipitated nanoparticles.

2.4. Preparation of the pH-sensitive nanosensors. A PAH polyelectrolyte layer conjugated with fluorescein was deposited onto the surface of the as synthesized Eu-doped $NaGd(WO_4)_2$ nanoparticles as follows: 500 µL of a poly(fluorescein isothiocyanate allylamine hydrochloride) solution (5 mg/mL, 0.05 M in NaCl, pH 6.5) was added to 150 µL of an aqueous dispersion containing 1.2 mg of the Eu:$NaGd(WO_4)_2$ nanoparticles. The resulting dispersion was sonicated in cold water for 5 minutes and then

shaken for 15 minutes. The so functionalized particles were centrifuged and washed three times with water. In the last washing, the supernatant had no color, indicating that the excess of reagents was completely removed. The PAH-fluorescein coated nanoparticles were finally dispersed in water at a final concentration of 2.4 mg/mL. For the pH sensing experiments, a 5-fold dilution of such dispersion in different buffer solutions was performed. Aqueous universal buffer solutions (pH = 3-12) were prepared by mixing appropriate volumes of 0.04 mol dm^{-3} phosphoric acid, 0.04 mol dm^{-3} boric acid, 0.04 mol dm^{-3} acetic acid and a 0.2 mol dm^{-3} sodium hydroxide.

2.5. Characterization: Particle shape was examined by transmission electron microscopy (TEM, Philips 200CM). For this, a droplet of an aqueous suspension of the sample was deposited on a copper grid coated with a transparent polymer and dried. Particle size was measured by counting several hundred of particles from the TEM micrographs, as well as by dynamic light scattering (DLS) measurements (Zetasizer NanoZS90, Malvern) conducted on aqueous suspensions (nanoparticles content = 0.2 mg cm^{-3}). The crystalline structure of the prepared particles was identified by X-ray diffraction (XRD, Panalytical X´Pert Pro with an X-Celerator detector). The crystallite size was estimated from the first XRD peak of the $NaGd(WO_4)_2$ (112) (2θ at 28.8º) by using the Scherrer formula. The infrared spectra (FTIR) of the nanoparticles diluted in KBr pellets were recorded in a Jasco FT/IR-6200 Fourier transform spectrometer. Thermogravimetric analysis (TGA) was performed in air at a heating rate of 10°C min^{-1}, using a Q600 TA Instrument. Zeta potential measurements for aqueous suspensions (pH= 7) were carried out in a Malvern Zetasizer Nano-ZS90 apparatus.

The excitation and emission spectra of the samples dispersed in Milli-Q water (0.15 mg cm^{-3}) were recorded in a Horiba Jobin Yvon spectrofluorimeter (Fluorolog FL3-11) equipped with a 450 W Xenon CW lamp, operating in the front face mode. This

equipment was also used to perform lifetime measurements with a pulsed xenon lamp. The decay curves were recorded on powder samples with an excitation wavelength of 254 nm (excitation slit = 4 nm) at an emission wavelength of 616 nm (emission slit = 1 nm). A time range of 11 ms was used. The fluorescence emission of aqueous suspensions containing PAH-fluorescein coated nanoparticles (0.5 mg cm^{-3}) was recorded at different pH values (from 3 to 11) under two excitation wavelengths (250 and 490 nm). The ratiometric analytical signal, i.e. fluorescence intensity corresponding to the fluorescein emission at 512 nm (under 490 nm excitation) divided by the fluorescence intensity associated with the Eu^{3+} cations at 611 nm (under 250 nm excitation) was calculated to study the pH response of the nanoparticles.

3. Results and Discussion

3.1. Nanoparticles synthesis and characterization

The synthesis of Eu:$NaGd(WO_4)_2$ nanoparticles was conducted through a homogeneous precipitation reaction at moderated temperature (120ºC) for 20 h, using sodium tungstate (Na_2WO_4) as source of both Na^+ and WO_4^{2-} anions. It is well known that to achieve a homogeneous precipitation process, the cations or anions involved in the solid phase formation must be released slowly and in a controlled manner into the solution.[29] Such controlled release may be carried out from precursors, which are able to liberate the precipitating ions on heating.[29] In our case, we selected for such purpose a Ln^{3+}-citrate complex formed in solution as a first step of the synthesis process, which has been shown to be successful for the synthesis of other lanthanide based nanostructures.[30-32] It is has been also well stablished that the formation of uniform particles by using this approach requires a rather precise reaction kinetic, which can be found through the proper adjustment of the reaction parameters. These include reagents concentrations,

temperature, aging time and also the nature of solvents, whose properties (viscosity and dielectric constant) affect the diffusion process involved in the solid phase formation and the possible aggregation behavior of the initially formed particles.[33] In this work, such effects were investigated using EG/H_2O mixtures as solvent.

The influence of different experimental conditions (reagent concentrations and EG/H_2O ratio) on the precipitation behavior and morphological characteristics of the particles synthesized according to the here reported procedure are summarized in Table 1. This table refers to the undoped system which was first addressed for simplicity. As observed, uniform particles, which show a spherical shape were only obtained under a very critical set of conditions involving a Gd^{3+} concentration of 0.05 mol dm^{-3}, a WO_4^{2-}/Gd^{3+} mol ratio = 2, a citrate/Gd^{3+} mol ratio = 2 and a EG/H_2O volumetric ratio = 4. The use of a lower citrate/Gd^{3+} mol ratio ($\leq$ 1) keeping constant the other experimental parameters, resulted in the instantaneous precipitation of heterogeneous particles suggesting that the Gd-citrate complex was not formed in this case, whereas no precipitation was detected when using a higher citrate concentration (citrate/Gd^{3+} = 4), which may due to a high thermal stability of the complex formed under these conditions. The decrease of the EG/H_2O ratio from 4/1 to 3/2 also resulted in a heterogeneous system while no precipitation took place for a solvent richer in EG. This behavior might be connected with the increase of viscosity resulting from the increase in the EG content of the solvent mixture which should slow down the reaction rate. Finally, precipitation was not observed when decreasing the Gd^{3+} concentration from 0.05 to 0.02 mol dm^{-3}. However, the increase of this magnitude or the WO_4^{2-}/Gd^{3+} ratio gave rise to heterogeneous particles probably due to the increase of the reaction rate expected as increasing the reagents concentration.

The uniform nanospheres (Fig. 1A) obtained as above described showed a mean diameter of 88 nm (standard deviation = 17) as determined from the TEM micrographs. DLS

measurement conducted for aqueous suspensions (pH = 7) of these nanoparticles (Fig. 1B) gave a mean hydrodynamic diameter of 120 nm, which is only slightly higher than that obtained from the TEM micrograph indicating that they were free of aggregation. This behavior can be justified in view of the high value of the zeta potential (- 39 mV) measured for such dispersions, which should involve a high repulsive interaction between the colloidal nanospheres. X-ray diffraction (Fig. 2A) indicated that such nanoparticles consisted of tetragonal $NaGd(WO_4)_2$. The crystal size estimated from this pattern was much smaller (10 nm) than particle size suggesting that the nanospheres are composed by crystalline subunits. FTIR gave more information on the composition of the particles. Thus, the recorded spectrum (Fig. 2B) displayed the bands characteristics of the WO_4^{2-} lattice vibrations (< 1000 cm^{-1})[7] along with two broad features centered at 3400 and 1580 cm^{-1} due to absorbed water. Some additional bands in the 3100-2800 and the 1600-1400 cm^{-1} regions were also detected, which must be attributed to vibration modes of C-H and carboxylate groups, respectively, coming from citrate anions adsorbed on the nanoparticles surface.[30] These anions may act as capping agents controlling particle growth and might also contribute to the higher degree of dispersion of our nanoparticles due to their well-known dispersing ability.

For the synthesis of Eu-doped nanophosphors, we followed a similar procedure to that driving to the uniform particles shown in Fig. 1A but adding the desired amount of Eu^{3+} to the starting solutions and keeping the total Ln concentration constant (0.05 mol dm^{-3}). Several doping levels were assayed in order to optimize the optical properties of such nanophosphors. It was found that the presence of Eu cations in the precipitating solutions had no effect on the particle morphology (Fig. 3), although a small increase in particle size was detected as increasing the amount of Eu^{3+} (Table 2). It must be mentioned that in recent works, several authors have observed that for different rare earth compounds

synthesized through precipitation processes, particle size can be modified by doping with other rare earths cations.[34] This behavior has been justified on the basis of the nucleation energy change induced by the dopant cation, which modifies the precipitation kinetics. As a consequence, the number of nuclei generated should vary, which must produce changes in the size that they will reach at the end of the growth stage.[34]

Hydrodynamic diameter values determined for aqueous dispersions of the doped particles were close to the particle size as determined from TEM (Table 2) indicating the absence of aggregation of the doped particles as it was also observed for the undoped system. The composition of the nanoparticles in terms of their Eu/Eu+Gd mol ratio as determined by ICP was in agreement with the nominal composition (Table 2) indicating the successful incorporation of Eu cations into the $NaGd(WO_4)_2$ matrix. XRD diffraction patterns of the doped particles (Fig. 4) and the values of crystal size obtained from them (Table 2) were also similar to those of the undoped system indicating that the doped particles also crystallized into the tetragonal $NaGd(WO_4)_2$ structure and were polycrystalline. FTIR analyses revealed the presence of citrated anions adsorbed on the doped nanoparticles surface since the FTIR spectra of all doped samples (not shown) were indistinguishable from that of the undoped system (Fig. 2B).

The excitation spectra of all doped samples, obtained by monitoring the most intense emission band expected for Eu^{3+} in this matrix (616 nm),[9] were similar to that shown in Fig. 5A, which correspond to the as-synthesized Eu(6%):$NaGd(WO_4)_2$ nanoparticles, chosen as a representative example. As observed, this spectrum presented a strong broad feature whose maximum intensity was detected at the minimum wavelength detected by the here used spectrofluorimeter (250 nm). This band has been ascribed to a charge transfer (CTB) transition within the WO_4^{2-} groups and the subsequent energy transfer

(ET) process from the excited levels of WO_4^{2-} anions to the Eu^{3+} cations.[35] It has been also reported that this broad feature also includes a Eu-O CTB and a narrow and much weaker band due to an ET process from the Gd to Eu cations,[35] which should appear at ~277 nm.[35] The spectrum also displayed some bands at > 300 nm (the most intense appeared at 393 nm) (inset in Fig. 5A), which correspond to the direct excitation of Eu^{3+} and are due to the f-f electronic transitions characteristics of these cations.[35] The much lower intensity of the later features when compared to that of the ET band indicates that the most effective excitation pathway for this phosphor is through the WO_4^{2-} groups. Irrespective of the Eu content, the emission spectra obtained by so doing (λ_{ex} = 250 nm) showed the expected bands associated with the electronic transitions from the $^5D_0$ to the ^7F_J (J =0, 1, 2, 3, and 4) levels of Eu^{3+} (Fig. 5B).[35] Among them, the one due to the $^5D_0$-$^7F_2$ transition (616 nm) clearly shows the highest intensity, which indicates that the Eu^{3+} ions are located in an environment of low symmetry within the crystalline tungstate matrix[35] and is the cause of the a high red color purity of the nanophosphors emissions, as observed in the inset in Fig. 5B.

The emission spectra recorded for the other prepared nanophosphors having different doping levels have been also included in Fig. 5B. From this figure, it is also clear that the increase of the Eu doping level from 3% to 12% resulted in an increase of the intensity of the emissions due to the increase in the number of emission centers. However, for a higher Eu^{3+} content (18%), the luminescence intensity remained almost constant suggesting the presence of the well-known concentration quenching effect. Measurements of the lifetime values associated with the Eu^{3+} luminescence were conducted to gain more information on such quenching process.

The decay curves corresponding to the $^5D_0 \rightarrow {}^7F_2$ transition of Eu^{3+} (616 nm) obtained after pulsed excitation at λ_{ex}=250 nm, for samples containing different doping levels are

shown in Fig. 6A. In all cases, the curves could be fitted using a bi-exponential temporal dependence according to Equation (1):

$$I(t) = I_{01}\exp(-t/\tau_1) + I_{02}\exp(-t/\tau_2) \qquad (1)$$

where I(t) is the luminescence intensity, t is the time after excitation, and τ_i (i = 1, 2) is the decay time of the *i* component, with intensity I_{0i}. The corresponding fitting parameters are summarized in Table 3 along with the average decay times, $<\tau>$, defined as:

$$\langle\tau\rangle = \frac{\int_{t_0}^{t_f} tI(t)dt}{\int_{t_0}^{t_f} I(t)dt} = \left(\tau_1^2 I_1 + \tau_2^2 I_2\right)/\left(\tau_1 I_1 + \tau_2 I_2\right) \qquad (2)$$

The shorter lifetime values are associated with the decay time of the active ions located near the particles surface, where the presence of impurities and solvent molecules (such as citrate anions and water, as revealed by FTIR in our case) led to the luminescence quenching through multiphononic processes.[36] The long lifetime values, which are dominant (I_{01}= 60-65%) for all samples (Table 3), can be assigned to the decay time of the Eu^{3+} ions located in the nanoparticles bulk, and therefore, not affected by surface effects,[33] As observed in Fig. 6B, the shorter lifetime values, did not show significant variations with the Eu content. However, although the values for the long lifetime were similar for the samples with lower Eu content (3-6% Eu) (the small variation observed was within the experimental error), those for the particles containing 12% and 18% Eu clearly decreased. The average lifetime showed a similar behavior with the Eu^{3+} doping level, confirming that a concentration quenching effect is present at Eu contents ≥12%. It must be mentioned that the larger average lifetime values (1.1-1 ms) obtained for our samples (3-6% Eu) were much higher than those reported in the literature for tetragonal Eu:$NaGd(WO_4)_2$ phosphors (≤ 0.56 ms)[37-38] which might be an indication of a higher luminescence efficiency in our nanoparticles.

For further studies, we selected the sample with an europium doping level of 6%, which is that with the more intense emissions among those with highest lifetime value (3-6% Eu) and could be then considered as the optimum system.

3.2. pH sensing

The originally negative charged citrate-capped Eu(6%):$NaGd(WO_4)_2$ nanoparticles were coated with the positively charged PAH polyelectrolyte layer conjugated with fluorescein by following a strategy similar to the Layer-by-Layer (LbL) approach. This method of functionalization is based on the electrostatic deposition of polyelectrolyte layers with alternating charge on the surface of the particles.[39] After this treatment, the nanoparticles showed orange color, suggesting the presence of fluorescein on their surface. Such suggestion was confirmed by the surface charge reversal (+21 mV at pH 7 after coating vs. -39 mV before coating) observed after the coating process. The hydrodynamic diameter obtained by DLS for the coated nanophosphors was very similar (127 nm) to that of the untreated particles (139 nm) (Table 2) indicating that no significant particle agglomeration took place as a consequence of the coating experiment. An estimation of the amount of PAH and fluorescein on the surface of the PAH-Fluorescein coated NPs was obtained from thermogravimetry (TG) analysis (Fig. 7). For the as synthesized sample, a weigh loss of around 4.7 % was observed at temperatures below 250 °C, which can be associated with the elimination of absorbed water. From this temperature to 500°C, the observed loss of about 4.8 % should be connected with the decomposition of the adsorbed citrate molecules. The PAH-fluorescein coated sample shows a similar behavior, but with a higher weight loss between 200 and 500 °C (around 6.4 %). This weight loss difference (1.6 %) should be due to the presence of the PAH-fluorescein coating layer. Based on these TG data, the amount of fluorescein associated with every

NP can be estimated, resulting in around 21100 molecules of fluorescein per NP (detailed numbers can be found in the Supporting Information).

Changes of the fluorescence response of the PAH-fluorescein coated Eu (6%):$NaGd(WO_4)_2$ nanoparticles towards pH were evaluated over a wide pH range (pH = 3-12) recording independently the emission of the Eu^{3+} cations from the nanoparticle cores (excitation wavelength = 250 nm) and the emission of the fluorescein from the nanoparticle shells (excitation wavelength = 490 nm). The maximum emission of the Eu^{3+} cations at 616 nm was found to be insensitive to the pH value (Fig. 8A) and therefore could be used as reference. The fluorescein attached to the nanoparticles, which showed a broad emission band centered at 512 nm, exhibited a clear dependence with pH (Fig. 8A). Thus, a remarkable increase of the emission intensity (around four times) was observed when increasing pH from 4 to 10 (Fig. 8A). This behavior allowed using the ratiometric intensity at these two different emission wavelengths as analytical signal, which is advantageous in terms of accuracy and reliability, because errors associated with environmental variations, probe distribution, and instrumental performance are diminished. The sigmoidal response obtained from the calibration curve of the ratio between the emission intensities of the fluorescein and the Eu^{3+} cations and the pH (Fig. 8B) demonstrated that such particles can be used as pH sensors in the pH 4-10 range.

4. Conclusions

Uniform Eu-doped $NaGd(WO_4)_2$ nanospheres have been synthesized through a homogeneous precipitation process at low temperature (120ºC) from solutions in an ethylene glycol/water mixture (volumetric ratio = 4/1) containing sodium tungstate, lanthanide (Eu and Gd) nitrates and sodium citrate used as complexing agent. The obtained nanoparticles crystallized into the tetragonal structure, presented polycrystalline

character and contained citrate anions adsorbed on their surface. The europium content in such phosphors has been optimized through the analysis of the luminescence dynamics (lifetime measurements) finding that the optimum phosphor is that doped with a 6% Eu^{3+}. By coating this nanophosphor with fluorescein (pH-sensitive dye) through a layer-by-layer (LbL) approach, a wide range (4-10) ratiometric pH-sensitive sensor has been developed, which uses the pH insensitive emission of Eu^{3+} as reference.

ASSOCIATED CONTENT

Details on the procedure for the estimation of the amount of PAH and fluorescein on the surface of the PAH-Fluorescein coated NPs as obtained from thermogravimetry (TG) analysis data

Acknowledgments

This work has been supported by the Spanish Ministry of Economy and Competitiveness (MINECO) (MAT2014-54852-R) and CSIC (PIE 201460E005 and PIE 201560E056). AE acknowledges Junta de Andalucía (Spain) for a Talentia Postdoc Fellowship, co-financed by the European Union Seventh Framework Programme, grant agreement no 267226.

References

1 W. Yang, X. Li, D. Chi, H. Zhang and X. Li, *Nanotechnology*, 2014, **25** (48), 482001.

2 C.-H. Kim, I.-E. Kwon, C.-H. Park, Y.-J. Hwang, H.-S. Bae, B.-Y. Yu, C.-H. Pyun and G.-Y. Hong, *J. of Alloys and Compounds*, 2000, **331** (1), 33.

3 M. Shang, C. Li and J. Lin, *Chem. Soc. Rev.*, 2014, **43**, 1372.

4 H. Dong, S.-R. Du, X.-Y. Zheng, G.-M. Lyu, L.-D. Sun, L.-D. Li, P.-Z. Zhang, C. Zhang and C.-H. Yan, *Chem. Rev.*, 2015, **115** (19), 10725.

5 G. Blasse, *Materials Chemistry and Physics*, 1987, **16** (3-4), 201.

6 Z. Hou, Z. Cheng, G. Li, W. Wang, C. Peng, C. Li, P. Ma, D. Yang, X. Kang and J. Lin, *Nanoscale*, 2011, **3**, 1568.

7 F. Esteban-Betegón, C. Zaldo and C. Cascales, *Chem. Mater.*, 2010, **22** (7), 2315.

8 J. Liao, L. Nie, Q. Wang, S. Liu, H.-R. Wen and J. Wu, *RSC Adv.*, 2016, **6**, 35152.

9 Y. Liu, G. Liu, J. Wang, X. Dong and W. Yu, *Inorg. Chem.*, 2014, **53** (21), 11457.

10 H. N. Luitel, R. Chand, T. Torikai, M. Yada and T. Watari, *RSC Adv.*, 2015, **5**, 17034.

11 X. Duan and Y. Li, *Small*, 2013, **9** (9-10), 1521.

12 Z. J. Wang, Y. L. Zhang, J. P. Zhong, H. H. Yao, J. Wang, M. M. Wu and A. Meijerink, *Nanoscale*, 2016, **8**, 15486.

13 N. Feliu, J. Hühn, M. V. Zyuzin, S. Ashraf, D. Valdeperez, A. Masood, H. Said, A. Escudero, B. Pelaz, E. Gonzalez, M. A. C. Duarte, S. Roy, I. Chakraborty, M. L. Lim, S. Sjöqvist, P. Jungebluth and W. J. Parak, *Sci. Total Environ*, 2016, **568**, 819.

14 C. Carrillo-Carrión, A. Escudero and W. J. Parak, *Trends Anal. Chem.*, 2016, **84**, 84.

15 P. K. Harimech, R. Hartmann, J. Rejman, P. del Pino, P. Rivera-Gil and W. J. Parak, *J. Mater. Chem. B*, 2015, **3** (14), 2801.

16 J. E. Whitaker, R. P. Haugland and F. G. Prendergast, *Anal. Biochem.*, 1991, **194** (2), 330.

17 F. Zhang, Z. Ali, F. Amin, A. Feltz, M. Oheim and W. J. Parak, *ChemPhysChem*, 2010, **11** (3), 730.

18 M. Semmling, O. Kreft, A. Muñoz Javier, G. B. Sukhorukov, J. Käs and W. J. Parak, *Small*, 2008, **4** (10), 1763.

19 P. Rivera-Gil, M. Nazarenus, S. Ashraf and W. J. Parak, *Small*, 2012, **8** (6), 943.

20 F. Zhang, E. Lees, F. Amin, P. Rivera-Gil, F. Yang, P. Mulvaney and W. J. Parak, *Small*, 2011, **7** (22), 3113.

21 T. V. Esipova, X. Ye, J. E. Collins, S. Sakadžić, E. T. Mandeville, C. B. Murray and S. A. Vinogradov, *Proc. Natl. Acad. Sci.*, 2012, **109** (51), 20826.

22 R. V. Benjaminsen, H. Sun, J. R. Henriksen, N. M. Christensen, K. Almdal and T. L. Andresen, *ACS Nano*, 2011, **5** (7), 5864.

23 A. Escudero, C. Carrillo-Carrión, M. V. Zyuzin, S. Ashraf, R. Hartmann, N. O. Núñez, M. Ocaña and W. J. Parak, *Nanoscale*, 2016, **8** (24), 12221.

24 R. Sjöback, J. Nygren and M. Kubista, *Spectroc. Acta Pt. A-Molec. Biomolec. Spectr.*, 1995, **51** (6), L7.

25 X. Guan and Z. Su, *Polym. Adv. Technol.*, 2008, **19** (5), 385.

26 R. M. Fratila, S. G. Mitchell, P. del Pino, V. Grazu and J. M. de la Fuente, *Langmuir*, 2014, **30** (50), 15057.

27 G. B. Sukhorukov, D. V. Volodkin, A. M. Gunther, A. I. Petrov, D. B. Shenoy and H. Mohwald, *J. Mater. Chem.*, 2004, **14** (14), 2073.

28 S. Wilhelm, M. Kaiser, C. Wurth, J. Heiland, C. Carrillo-Carrion, V. Muhr, O. S. Wolfbeis and W. J. Parak, *Nanoscale*, 2015, **7** (4), 1403.

29 E. Matijević, *Chem. Mater.*, 1993, **5**, 412.

30 J. Zhao, Y. Sun, X. Kong, L. Tian, Y. Wang, T. L. Tu, J. Zhao and H. Zhang, *J. Phys. Chem. B.*, 2008, **112** (49), 15666.

31 N. O. Nuñez, S. Rodriguez-Liviano and M. Ocaña, *J. of Colloid and Interface Science*, 2010, **349** (2), 484.

32 M. Laguna, N. O. Nuñez, V. Rodriguez, E. Cantelar, G. Stepien, M. L. Garcia, J. M. de la Fuente and M. Ocaña, *Dalton Transactions*, 2016, **45** (41), 16354.

33 N. O. Nuñez, J. Sabek, J. García-Sevillano, E. Cantelar, A. Escudero and M. Ocaña, *Eur. J. Inorg. Chem.*, 2013, **2013** (8), 1301.

34 D. Chen and Y. Wang, *Nanoscale*, 2013, **5**, 4621.

35 Y. Wang, J. Tang, X. Huang and L. Jiang, *Journal of Rare Earths*, 2016, **34** (2), 118.

36 J. W. Stouwdam, M. Raudsepp and F. C. J. M. van Veggel, *Langmuir*, 2005, **21** (15), 7003.

37 J. Liao, H. You, B. Qiu, H.-R. Wen, R. Hong, W. You and Z. Xie, *Current Applied Physics*, 2011, **11** (3), 503.

38 P. A. Loiko, E. V. Vilejshikova, X. Mateos, J. M. Serres, V. I. Dashkevich, V. A. Orlovich, A. S. Yasukevich, N. V. Kuleshov, K. V. Yumashev, S. V. Grigoriev, S. M. Vatnik, S. N. Bagaev and A. A. Pavlyuk, *Optical Materials*, 2016, **57**, 1.

39 G. B. Sukhorukov, E. Donath, S. Davis, H. Lichtenfeld, F. Caruso, V. I. Popov and H. Möhwald, *Polym. Adv. Technol.*, 1998, **9** (10-11), 759.

Table 1. Particle shape and size (mean diameter) of the particles precipitated by aging at 120ºC for 20 h, solutions containing different reagents amount in different EG/H_2O water mixtures. The standard deviation corresponding to the size measurement is shown in parenthesis.

$[Gd^{3+}]$ (mol dm^{-3})	WO_4^{2-}/Gd^{3+} (mol ratio)	Citrate/Gd^{3+} (mol ratio)	EG/H_2O ratio (by vol.)	Shape	Size (nm)
0.05	2	4	4/1	No precipitation	
0.05	2	2	4/1	Spheres	88 (17)
0.05	2	1	4/1	Heterogenous	
0,05	2	2	5/0	No precipitation	
0.05	2	2	4.5/0.5	No precipitation	
0.05	2	2	3/2	Heterogeneous	
0.02	2	2	4/1	No precipitation	
0.10	2	2	4/1	Heterogeneous	
0.05	5	2	4/1	Heterogeneous	

Table 2. Nominal and experimental (ICP) Eu/(Eu+Gd) mol ratio, particle size, hydrodynamic diameter and crystal size measured for the Eu-doped $NaGd(WO_4)_2$ samples. The standard deviation corresponding to the particle size measurements is shown in parenthesis

Eu/(Eu+Gd) Nominal (%)	Eu/(Eu+Gd) ICP (%)	Diameter (nm)	Hydrodynamic diameter (nm)	Crystallite size (nm)
3	2.8	117 (10)	145	11
6	6.5	119 (21)	139	13
12	13.6	131 (11)	151	13
18	20.2	134 (16)	158	12

Table 3. Fitting parameters of the bi-exponential temporal dependence for the luminescence decay curves of the Eu^{3+}-doped $NaGdWO_4$ phosphors recorded at the dominant emission (616 nm) of the Eu^{3+} ion (experimental error = 6%).

Eu/(Eu+Gd) Nominal (%)	**I_{01}**	**τ_1 (ms)**	**I_{02}**	**τ_2 (ms)**	**$<\tau>$ (ms)**
3	61	1.243	39	0.397	1.097
6	61	1.140	39	0.426	1.002
12	64	0.968	36	0.396	0.860
18	67	0.894	33	0.359	0.806

List of figures

Fig. 1 (A) TEM image of the particles obtained by aging at 120°C for 20 h, a solution in ethylene glycol/water (4/1 by vol.) containing $Gd(NO_3)_3$ (0.05 mol dm^{-3}), Na_3Cit (0.1 mol dm^{-3}) and Na_2WO_4 (0.1 mol dm^{-3}). Inset shows a high magnification image of a single nanoparticle. (B) Size (hydrodynamic diameter) distribution obtained from DLS measurements carried out for aqueous dispersions of these particles at pH = 7.

Fig. 2 (A) X-ray diffraction pattern obtained for the particles shown in Figure 1A. The PDF file for tetragonal $NaGd(WO_4)_2$ is also included. (B) Infrared spectra obtained for the same sample.

Fig. 3 TEM images of the particles obtained by aging at 120°C for 20 h, solutions in ethylene glycol/water (4/1 by vol.) containing $Gd(NO_3)_3$, Na_3Cit (0.1 mol dm^{-3}), Na_2WO_4 (0.1 mol dm^{-3}) and $Eu(NO_3)_3$ with different Eu content (Eu/(Eu+Gd) mol ratio).

Fig. 4 X-ray diffraction patterns obtained for the as-synthesized $NaGd(WO_4)_2$ particles doped with different amounts of europium (Eu/(Eu+Gd) mol ratio).

Fig. 5 (A) Excitation spectrum (λ_{em}= 615 nm) recorded for the as-synthesized Eu(6%):$NaGd(WO_4)_2$ particles. (B) Emision spectra (λ_{ex}= 250 nm) recorded for the as-synthesized Eu:$NaGd(WO_4)_2$ particles doped with different amounts of Eu. Inset in (B) shows a photograph of the particles in water suspension taken under UV illumination at λ = 254 nm.

Fig. 6 (A) Temporal evolution of the $^5D_0 - ^7F_1$ luminescence for the as-synthesized Eu:$NaGd(WO_4)_2$ phosphors doped with different amounts of Eu^{3+} (λ_{ex} = 250 nm). Solid lines correspond to the fitting of the experimental data using eq. 1 with the parameters given in Table 3. Evolution of the partial (B) and average (C) lifetimes with Eu^{3+} doping level.

Fig. 7 TG analysis of the as-synthesized Eu(6%):$NaGd(WO_4)_2$ NPs before (black line) and after (red line) coating with PAH-fluorescein.

Fig. 8 (A) Emission spectra of the as-synthesized Eu(6%):$NaGd(WO_4)_2$ NPs coated with poly(fluorescein isothiocyanate allylamine hydrochloride) at pH 4 (blue), 7 (green), and 12 (red). Emission of Eu^{3+} (right part) was collected with excitation at λ_{ex} = 250 nm, while λ_{ex} for fluorescein was 490 nm (emission on the left part). All the spectra are represented with the same scale. (B) Intensity ratio of the fluorescein (maximum λ_{em} = 512 nm, λ_{ex} = 490 nm) and Eu^{3+} (λ_{em} = 611 nm, λ_{ex} = 250 nm) emissions at different pH values. The error bars are smaller than the size of the symbols.

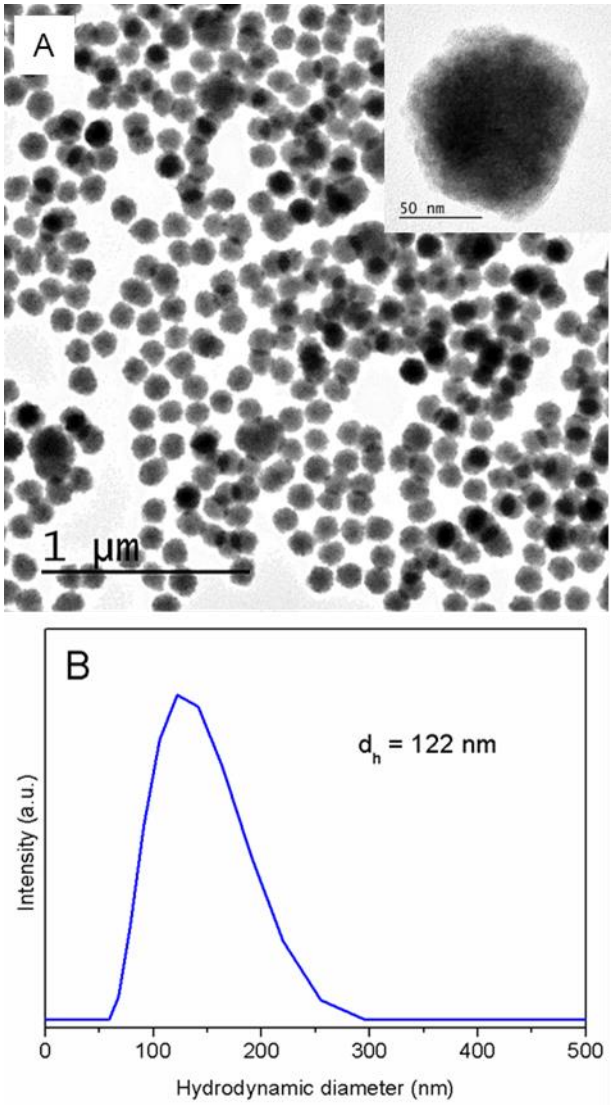
A
50 nm
1 µm
B
d_h = 122 nm
Intensity (a.u.)
0
100
200
300
400
500
Hydrodynamic diameter (nm)

Fig. 1

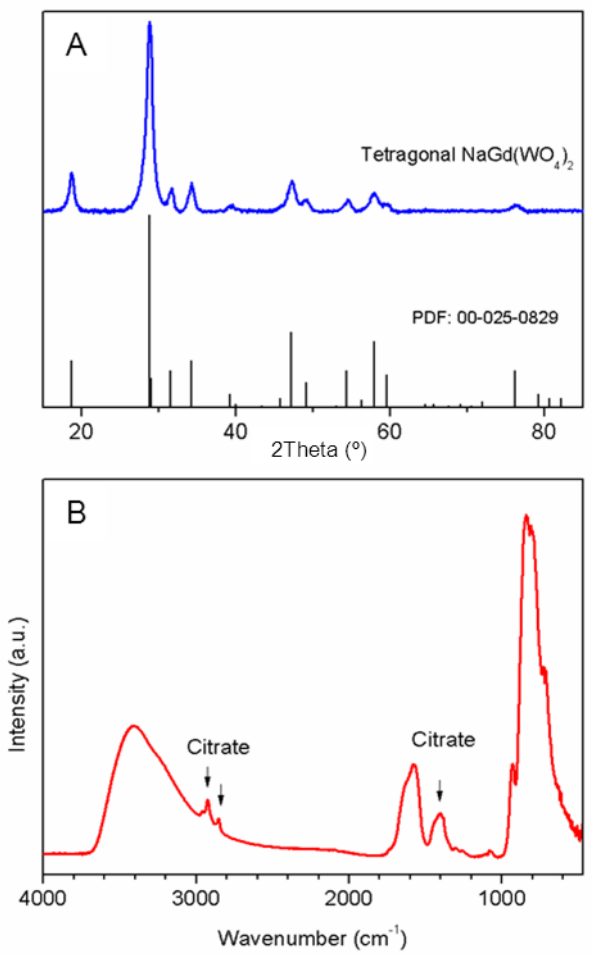
A
Tetragonal NaGd(WO4)2
PDF: 00-025-0829
20
40
60
80
2Theta (°)
B
Intensity (a.u.)
Citrate
Citrate
4000
3000
2000
1000
Wavenumber (cm-1)

Fig. 2

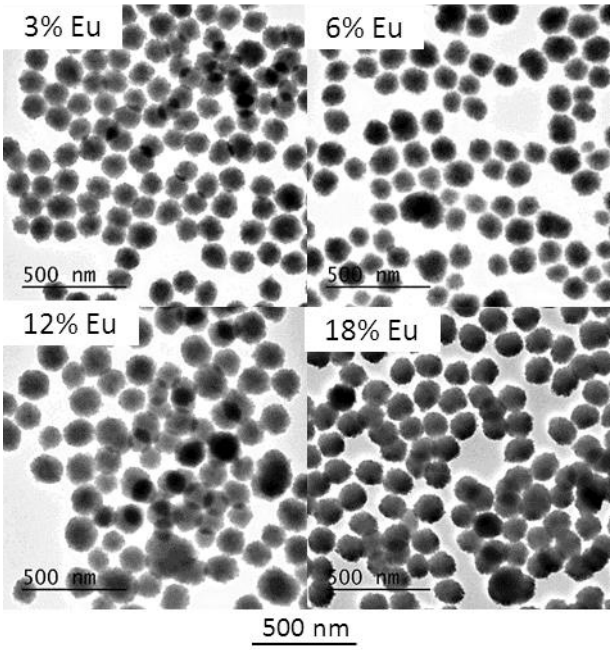
3% Eu
6% Eu
12% Eu
18% Eu
500 nm
500 nm
500 nm
500 nm
500 nm

Fig. 3

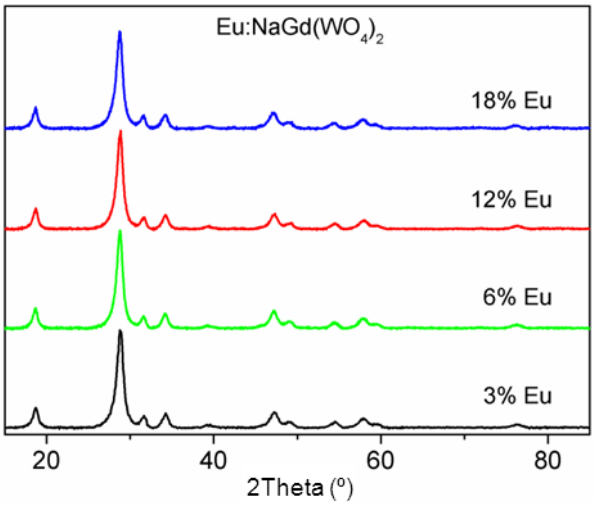
Eu:NaGd(WO4)2
18% Eu
12% Eu
6% Eu
3% Eu
20
40
60
80
2Theta (°)

Fig. 4

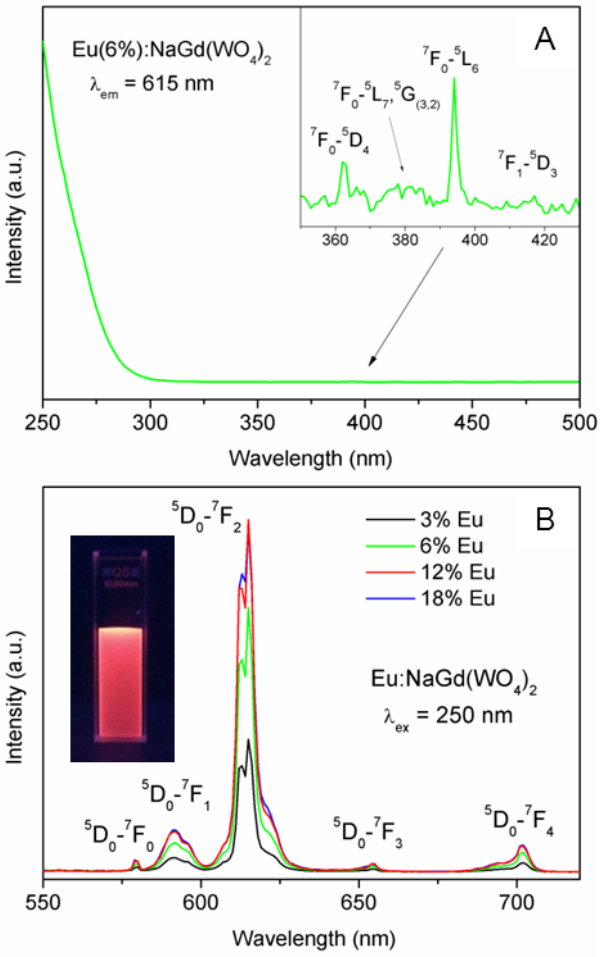
Eu(6%):NaGd(WO4)2
λem = 615 nm
A
7F0-5L6
7F0-5L7, 5G(3,2)
7F0-5D4
7F1-5D3
360
380
400
420
Intensity (a.u.)
250
300
350
400
450
500
Wavelength (nm)
5D0-7F2
3% Eu
6% Eu
12% Eu
18% Eu
B
Eu:NaGd(WO4)2
λex = 250 nm
5D0-7F1
5D0-7F0
5D0-7F3
5D0-7F4
Intensity (a.u.)
550
600
650
700
Wavelength (nm)

Fig. 5

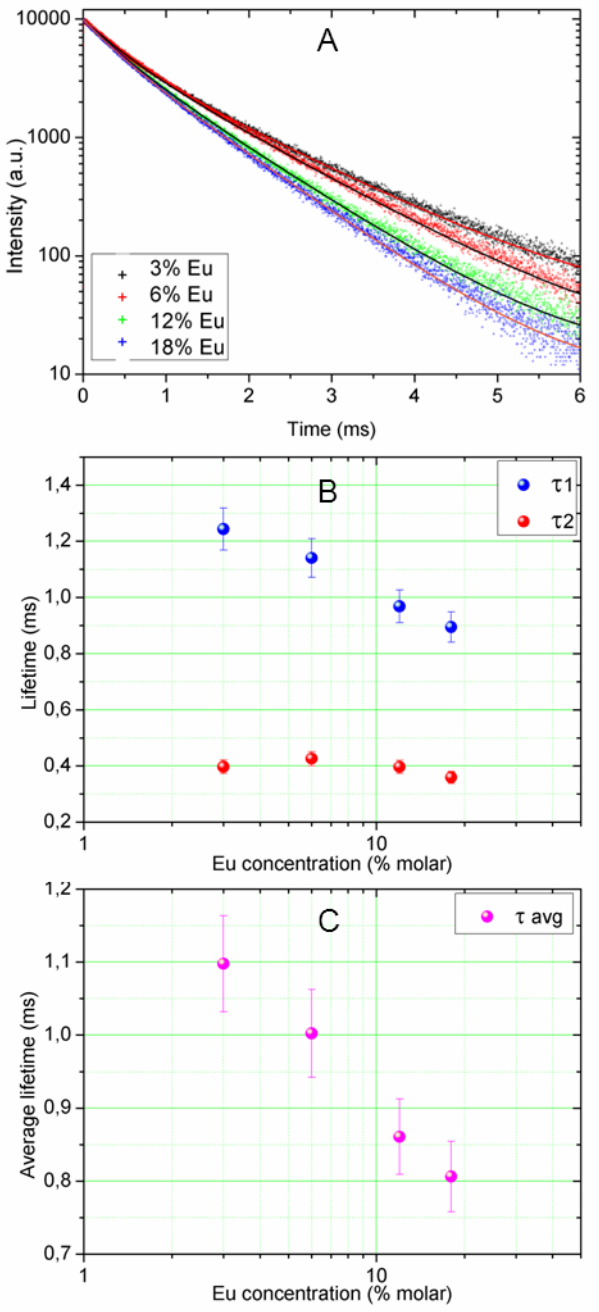
A
Intensity (a.u.)
Time (ms)
3% Eu
6% Eu
12% Eu
18% Eu
B
τ1
τ2
Lifetime (ms)
Eu concentration (% molar)
C
τ avg
Average lifetime (ms)
Eu concentration (% molar)

Fig. 6

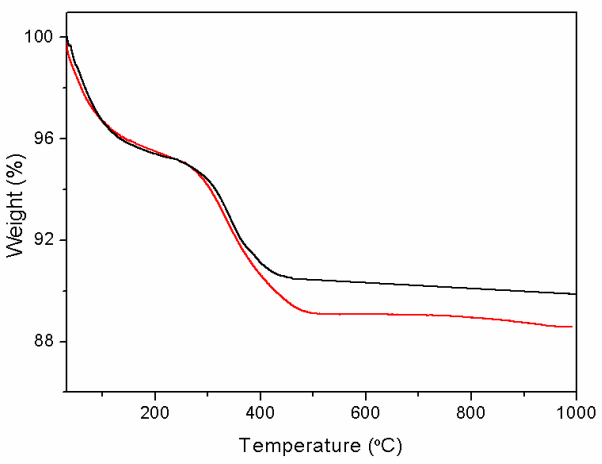
100
96
92
88
Weight (%)
200
400
600
800
1000
Temperature (°C)

Fig. 7

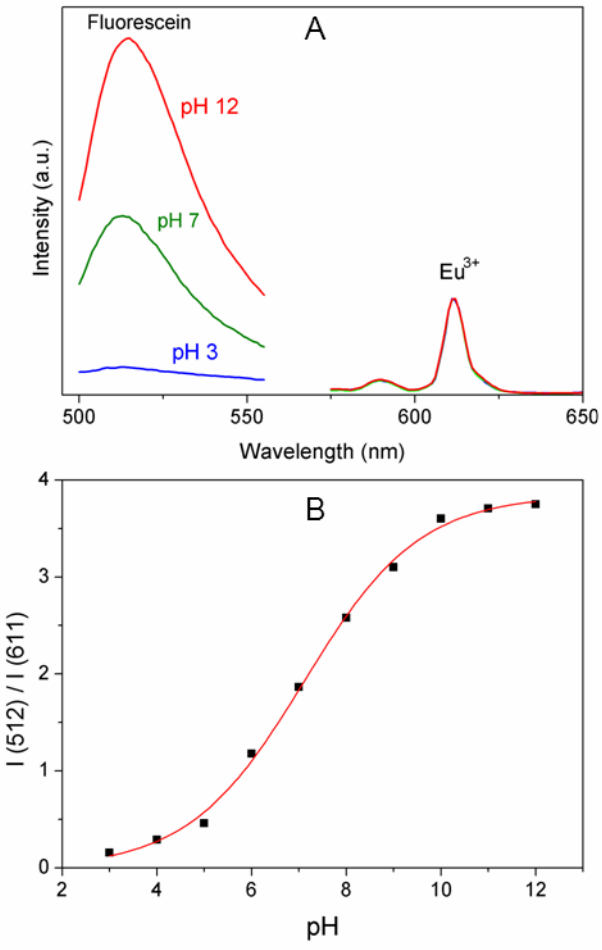
Fluorescein
A
pH 12
pH 7
pH 3
Eu3+
Intensity (a.u.)
500
550
600
650
Wavelength (nm)
B
I (512) / I (611)
0
1
2
3
4
2
4
6
8
10
12
pH

Fig. 8

Graphical Abstract